A Universal Platform for Selective Phase Growth and Precise-layer Control in $MoTe_2$

James P. Fraser,[a] Liudvika Masaityte,[a] Jingyi Zhang,[b] Stacey Laing,[c] Juan Carlos Moreno-López,[d] Adam McKenzie,[a] Jessica C. McGlynn,[a] Vishal Panchal,[e] Duncan Graham,[c] Olga Kazakova,[e] Thomas Pichler,[d] Donald A. MacLaren,[f] David A.J. Moran,[b] Alexey Y. Ganin[a,*]

a) *School of Chemistry, University of Glasgow, Glasgow, G12 8QQ, United Kingdom*
b) *School of Engineering, University of Glasgow, Glasgow, G12 8LT, United Kingdom*
c) *Department of Pure and Applied Chemistry, University of Strathclyde, 99 George Street, Glasgow, G1 1RD, United Kingdom*
d) *University of Vienna, Faculty of Physics, Boltzmanngasse 5, A-1090, Vienna, Austria*
e) *National Physical Laboratory, Teddington, TW11 0LW, United Kingdom*
f) *SUPA, School of Physics and Astronomy, University of Glasgow, Glasgow G12 8QQ, UK*

Abstract

Minor structural changes in transition metal dichalcogenides can have dramatic effects on their electronic properties. This makes the quest for key parameters that can enable a selective choice between the competing metallic and semiconducting phases in the 2D $MoTe_2$ system compelling. Herein, we report the optimal condition at which the choice of the initial seed layer dictates the type of crystal structure of atomically-thin $MoTe_2$ films grown by chemical vapour deposition (CVD). When Mo metal is used as a seed layer, phase-pure semiconducting 2H-$MoTe_2$ is the only product. Conversely, MoO_3 leads to the preferential growth of phase-pure metallic 1T'-$MoTe_2$. The control over phase growth allows for simultaneous deposition of both 2H-$MoTe_2$ and 1T'-$MoTe_2$ phases on a single substrate during one CVD reaction. Furthermore, Rhodamine 6G dye can be detected using few-layered 1T'-$MoTe_2$ films down to 5 nM concentration which is several orders of magnitude higher than the value observed for bulk 1T'-$MoTe_2$.

1. Introduction

Chemical vapour deposition (CVD) has become a key method for the universal growth of high-quality atomically-thin transition metal dichalcogenides (TMDCs).[1–6] Cheap in design and scalable to industry level, even in basic laboratory settings, a CVD apparatus holds promise for a wider acceptance of TMDCs in future applications.[4,7–11] While MoS_2 and $MoSe_2$ few-layered films grown by CVD tend to invariably display only hexagonal structures, the less prominent $MoTe_2$ occurs in two polymorphic modifications. The hexagonal (2H-$MoTe_2$) polymorph (Figure 1a) in bulk form is an indirect-gap semiconductor but thinning it down to few-layers leads to the emergence of a direct bandgap of 1.1 eV.[12] This bandgap opening is accompanied by a strong photoluminescence signal in the near IR region (similar to Si), which makes 2H-$MoTe_2$ a viable candidate for optoelectronic devices.[10,13–15] Prototype photodetectors based on few-layered 2H-$MoTe_2$ have been suggested to become a future integrative part of silicon photonic applications.[10,16,17] Conversely, the monoclinic

1T'-$MoTe_2$ polymorph (Figure 1b) is a Weyl semi-metal in the bulk form. Since the discovery of topological superconductivity and large magnetoresistance in this compound it has been the subject of comprehensive fundamental research.[18–21] In addition, 1T'-$MoTe_2$ has been highlighted as an emerging energy material with applications ranging from photovoltaic cells to hydrogen evolution catalysis.[22–25] Furthermore, few-layered 1T'-$MoTe_2$ may become a promising sensing platform enabled through its ability to suppress fluorescence signals which often prevents reliable detection of Raman scattering from negligible traces of molecules.[26]

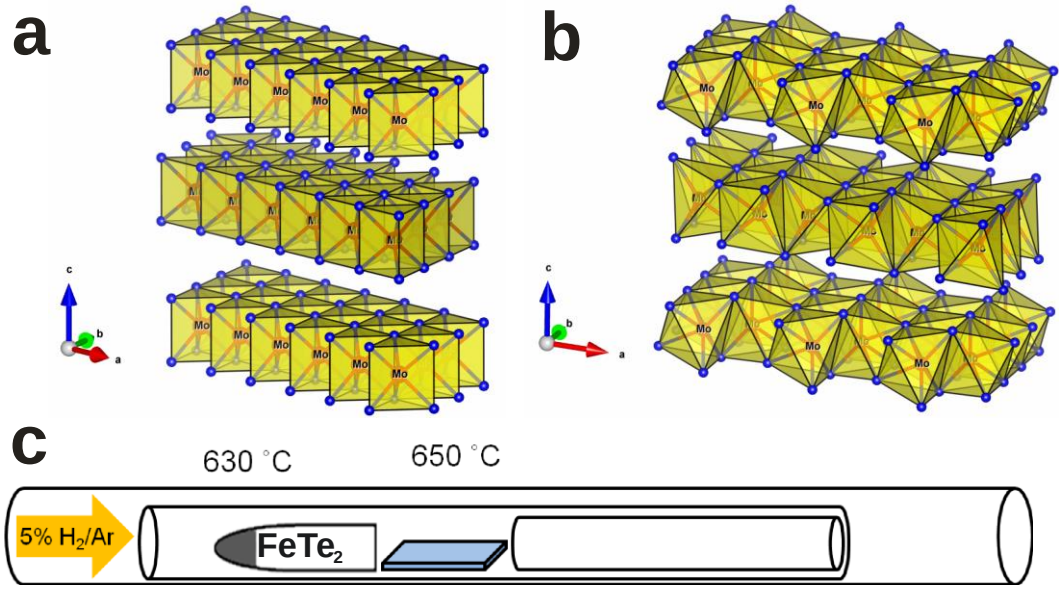

Figure 1. Crystal structure and polyhedral coordination of 3-layered hexagonal 2H-$MoTe_2$ (a) and monoclinic 1T'-$MoTe_2$ (b); A schematic of the CVD setup employed in this work (c). The temperatures of 630 °C and 650 °C stand for the temperature of the precursor source and substrate respectively.

In this context, polymorphism in $MoTe_2$ presents an interesting opportunity to exploit the role of crystal structure on the electronic properties without the need for compositional change: a useful feature especially if the polymorphism can be controlled.[10,27] However, unlike MoS_2 and $MoSe_2$,[28,29] which rely on self-assembly by a van-der-Waals epitaxy (vdWE) process,[30,31] the low electronegativity of Te presents a significant challenge for the deposition of atomically thin $MoTe_2$ by CVD. Despite the recent encouraging attempts,[32,33] the tantalizing task of finding the ultimate set of empirically-determined parameters (gas flow rates, H_2/Ar ratio, substrate temperatures, heating/cooling rates), which can enable a controlled self-assembly of uniform and high-area $MoTe_2$ by vdWE remains elusive.

Direct tellurization CVD has emerged as a viable alternative to vdWE for achieving continuous and high-area growth of $MoTe_2$.[34–37] The process relies on a reaction (facilitated by the reductive flow of H_2) between Te vapour and an atomically thin seeding layer (commonly MoO_3 or Mo) pre-deposited on a substrate. However, the pronounced polymorphism in $MoTe_2$ makes the control of the reaction outcome extremely difficult. At deposition temperatures in excess of 600 ^oC, which are required for achieving high-quality products, both the semiconducting 2H-$MoTe_2$ and the semi-metallic 1T'-$MoTe_2$ polymorphs are in direct competition with each other at the substrate interface.[32] Through

optimisation of reaction conditions it is possible to induce growth of a specific polymorph: for example, high ramping and cooling rates tend to produce 1T'-$MoTe_2$ while slower cooling rates and lower reaction temperatures generally lead to 2H-$MoTe_2$. However, this implies that the simultaneous growth of both 1T'-$MoTe_2$ and 2H-$MoTe_2$ would be impossible to achieve on the same substrate in a single step when the same seed layer is used. In practice, a post-growth modification, patterning (which is then followed by a second CVD step) is required.[38] Multiple-step procedures appear unpractical from the future industrial applications point of view and therefore, finding a protocol for the preferential growth of both $MoTe_2$ polymorphs on a same substrate and through a single step procedure is important.

In this work, we report the growth of large-area and homogeneous films of few-layered 1T'- or 2H-$MoTe_2$ by CVD on SiO_2/Si and sapphire substrates using $FeTe_2$ precursor. We found that at the deposition temperature of 650 ^oC the outcome of CVD was governed by the nature of the seeding layer with MoO_3 yielding 1T'-$MoTe_2$ and Mo leading to 2H-$MoTe_2$. This allowed for the simultaneous growth of 1T'- and 2H-$MoTe_2$ to be achieved on the same substrate in a single CVD reaction and without any intermediate steps. This was evidenced by Raman spectroscopy, atomic force microscopy (AFM), X-ray photoelectron spectroscopy (XPS), transmission electron microscopy (TEM) and total colour difference microscopy techniques. Furthermore, few-layered films of the metallic 1T'-$MoTe_2$ phase showed sensing ability towards the detection of small molecules. Specifically, the common dye Rhodamine 6G (R6G) was detected down to a 5 nM concentration on few-layered films, which is a significant improvement when compared with bulk 1T'-$MoTe_2$.

2. Results and Discussion

CVD Growth of few-layered 2H-$MoTe_2$ using Mo seeding layers

A CVD system, shown in Figure 1c, was designed and implemented to minimize the effect of the turbulence of the gas flow within the reactor and to keep the reaction conditions as close to equilibrium as possible (see Experimental section).

Figure 2a shows a typical AFM image of the product obtained by conversion of a 1 nm thick Mo film (deposited by thermal sputtering, see Experimental Section) on a SiO_2/Si substrate at 650 ^oC using 30 mg $FeTe_2$ as a precursor. The height profile collected at the step-edge between the film and the substrate corresponds to 4.1 nm (Figure 2b). Based on the assumption (from the length of the *c*-parameter in $MoTe_2$) that a monolayer of $MoTe_2$ should be *ca*. 0.7 nm thick[23] we estimated that the resulting film corresponded to six $MoTe_2$ layers. A typical AFM image for the six-layered $MoTe_2$ across a scan area of 5 μm × 5 μm is shown in Figure 2c. The measured root mean square (RMS) surface roughness, R_q, value of 0.6 nm is in excellent agreement with the R_q = 0.6 nm observed on the initial 1 nm Mo film (Figure S1a, Supporting Information). It should also be mentioned that the roughness values obtained from the $MoTe_2$ films are only marginally higher than that measured on a SiO_2/Si substrate with R_q = 0.45 nm (Figure S1b, Supporting Information).

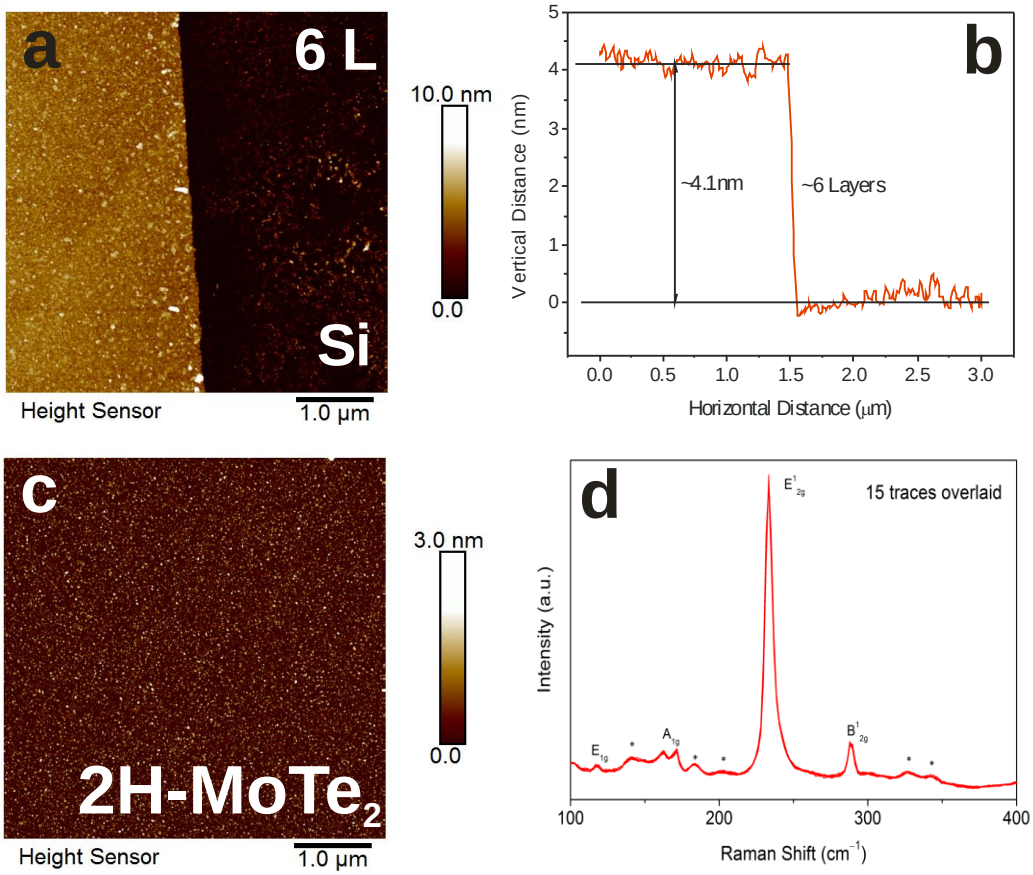

Figure 2. AFM measurement over the 5 μm x 5 μm area and a representative 2D topographic profile of the interface between few-layered 2H-$MoTe_2$ and SiO_2/Si substrate (a); the variation in height between the film and the substrate measured on a six-layered $MoTe_2$ film from Figure 2a (b); 2D topographic profile of a 5 μm x 5 μm area from a few-layered $MoTe_2$ film on SiO_2/Si substrate (c); A 532 nm Raman spectrum from a typical 6L 2H-$MoTe_2$ on 300 nm SiO_2/Si (d).

The in-plane E^1_{2g}-mode peak at *ca*. 234 cm^{-1} and a small out-of-plane A^1_g-mode peak at *ca.* 174 cm^{-1} in the Raman spectra of the film confirmed that the 2H-$MoTe_2$ polymorph is formed (Figure 2d) while the wide range spectra confirmed that the films are free from MoO_3 and MoO_2 (Figure S2, Supporting Information). The weak peaks at *ca*. 138 and 185 cm^{-1} are second-order Raman modes, as have been reported elsewhere.[39] The film is single-phase and uniform 2H-$MoTe_2$ across the entire substrate as evidenced from the perfect overlap of numerous spectra collected on the film at various locations across the substrate. Raman mapping based on the intensity of the E^1_{2g} mode confirms the uniformity of the CVD grown film (Figure S3, Supporting Information). In addition, the few-layered character of the grown 2H-$MoTe_2$ film was evident from the prominent phonon-active out-of-plane B^1_{2g} peak at *ca*. 289 cm^{-1} (Raman active in few-layered $MoTe_2$ but inactive in bulk).

The high-resolution X-ray photoelectron spectroscopy (XPS) spectra of the six-layered 2H-$MoTe_2$ on SiO_2/Si exhibit spin-orbit doublets for two oxidation states (Figure S4a, Supporting Information). The dominant doublet peaks at E_B = 228.12 eV and E_B = 231.2 eV can be assigned to Mo^{4+} $3d_{5/2}$ and Mo^{4+} $3d_{3/2}$ oxidation states for 2H-$MoTe_2$, respectively. The doublet upshifted to higher binding energies consists of a weak shoulder at E_B = 232.5 eV (Mo $3d_{5/2}$) and a broad feature at E_B = 235.71 eV (Mo

$3d_{3/2}$) which are consistent with the binding energies expected for the molybdenum oxidation states in MoO_3.[40,41] The oxidation peaks have been observed in other literature work and may originate from minute surface oxidation in ambient air during transfer to the XPS.[42] The tellurium 3d spectrum only displays a single doublet at E_B = 572.75 eV (Te $3d_{5/2}$) and E_B = 583.12 eV (Te $3d_{3/2}$) corresponding to $MoTe_2$ only (Figure S4b, Supporting Information). In addition, by comparing our measurements with reference values,[43] an upshift to higher binding energies of 0.12 eV for Mo $3d_{5/2}$ and a downshift of 0.35 eV for Te $3d_{5/2}$ peaks are observed, suggesting a net electron transfer from Mo to Te atoms. This is in line with expectation given the very small difference in electronegativity between Mo and Te ($\Delta\chi_{Te\text{-}Mo}$ = 0.3). In the survey spectrum, the Si peak arising from the substrate indicates that the beam penetrated the film down to the SiO_2/Si substrate. Since there is no evidence of Mo-metal bands in the high resolution XPS, this suggests that the Mo seeding layer was completely converted into $MoTe_2$ (Figure S4c, Supporting Information).

Transmission electron microscopy (TEM) was used to assess the crystallinity of a six-layered film transferred onto Au grids (Figure S5a, Supporting Information). The selected area diffraction confirmed the flake's polycrystallinity, which manifested as a sequence of diffraction rings rather than spots. At higher magnification the crystal structure is evident (Figure S5b, Supporting Information), including a moiré fringe effect between crystal layers lying towards the centre of the image, and indicating a polycrystalline structure that is confirmed by a Fourier transform with multiple sets of hexagonal spots. Energy Dispersive X-ray Spectroscopy spectrum is dominated by Mo, Te and Au (support grid) peaks (Figure S6, Supporting Information). Very weak Fe, C, Al and Si peaks are visible, at trace levels consistent with secondary scattering within the microscope.

Since the spectroscopy and microscopy data confirmed the nature of the films grown on SiO_2/Si, we additionally tested the method by growing $MoTe_2$ on a sapphire substrate. The positions and relative intensities of the peaks in the Raman spectra for the 6-layers film grown on a sapphire substrate is similar with the films deposited on SiO_2/Si. However, the absolute peak intensities were found to be weaker relative to the base line (Figure S7, Supporting Information). For example, the peak associated with the E_{1g} mode is unresolved due to the higher background. The subdued intensities are due to the transparency of the sapphire substrate to laser light,[39] which is in line with the previous observations for a 2.1 nm $MoTe_2$ film obtained on sapphire by physical vapour deposition.[44]

Controlled Growth of 2H-$MoTe_2$ with different thicknesses

To the best of our knowledge all previous reports on $MoTe_2$ have been focused on one-off few-layered samples while no reports are available where the films with different thicknesses can be grown in the same CVD setup. Therefore, we carried out the deposition process with the reaction parameters kept identical except for the thickness of the seeding Mo films. We deposited five Mo films (with 0.75, 1, 1.25, 1.5 and 1.75 nm thicknesses) by thermal sputtering and then converted them into $MoTe_2$.

The graph in Figure 3a shows the correlation between the thicknesses of the initial Mo film and the thickness of the resulting $MoTe_2$ as measured by AFM. The relevant 2D topological AFM images of

the interface between the films and the substrates are shown in Figure S8 while the height profiles for the films studied are summarized in Figure S9.

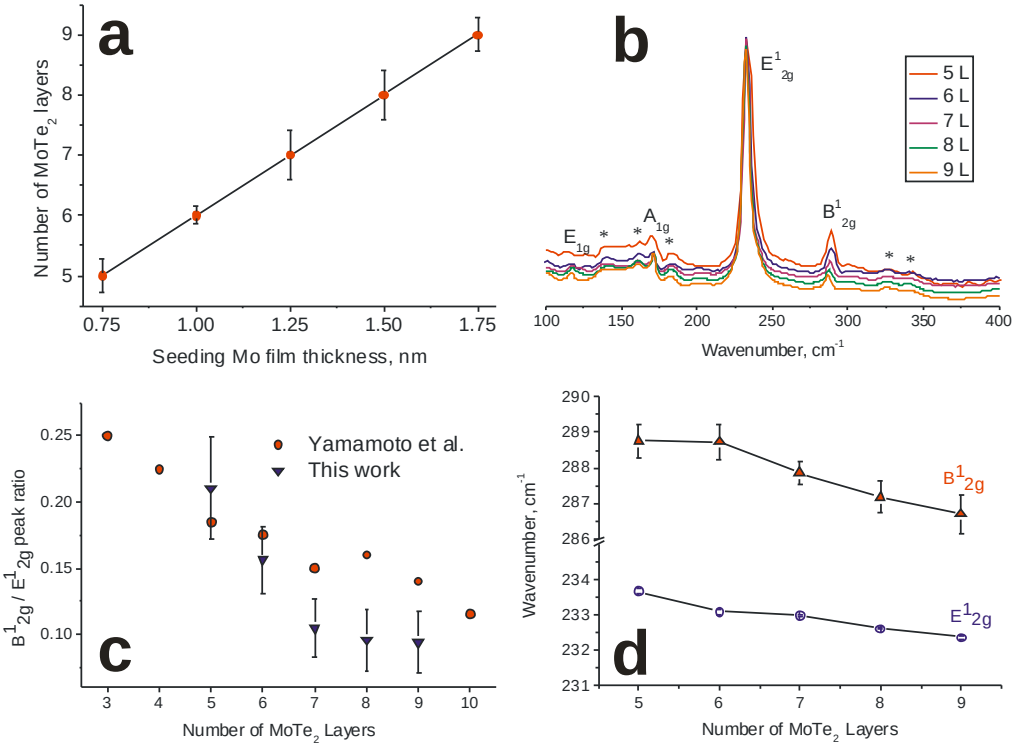

Figure 3. The correlation between the thickness of the thermally evaporated Mo film and the resulting few-layered $MoTe_2$ on 300 nm SiO_2/Si substrate (a); 532 nm Raman spectra depending on number of layers in few-layered 2H-$MoTe_2$ on 300 nm SiO_2/Si substrates. The spectra were shifted along *y*-axis for clarity. The modes associated with 2H-$MoTe_2$ are labelled and second order peaks are marked with * (b); Raman data assessment of B^1_{2g}/E^1_{2g} ratio for $MoTe_2$ films on 300 nm SiO_2/Si depending on the number of layers (blue triangles). The data (red circles) for exfoliated $MoTe_2$ samples adopted from Ref. [45] are plotted for comparison (c); Raman data assessment of the positions of B^1_{2g} and E^1_{2g} peaks depending upon the number of layers (d).

It is evident that the number of $MoTe_2$ layers (as before, under assumption that 1 $MoTe_2$ layer corresponds to *ca.* 0.7 nm) follows a clear trend line with the increase in the thickness of the initial Mo film. Conversely, there is no trend in the roughness of the films with increased thickness (Figure S10, Supporting Information) suggesting that the produced films are similar in terms of their morphologies, as also can be seen from the 2D topographical images depending on film thicknesses (Figure S11, Supporting Information). The AFM measurements confirmed that the samples at the studied thicknesses showed root mean square (RMS) surface roughness (R_q) values below 1 nm, thus, indicating that the surfaces of the films were smooth and uniform and comparable with the original Mo seeding layer. The similarity of morphologies suggests an isomorphic transformation of the molybdenum layer into $MoTe_2$. This is contrary to recent literature work that showed a substantial increase in the surface roughness of 2H-$MoTe_2$ compared with the initial Mo film when elemental Te was used.[35] We explain that the quality of the films is retained due to slow heating and cooling rates

of 5 ^{o}C min^{-1}, which were possible to apply due to the low vapour pressure of Te over the $FeTe_2$ precursor or/and lower Te^{-2} oxidation state. The slow rates may have helped to obtain smooth films by suppressing any differences in thermal coefficients between film and substrate, which would otherwise lead to rupturing of the film.

Figure 3b shows the 532 nm laser Raman spectra collected on a range of 2H-$MoTe_2$ films with a different number of layers. Earlier work on exfoliated flakes of 2H-$MoTe_2$ has shown that the B^1_{2g}/E^1_{2g} peak intensity ratio could be a useful parameter for rapid evaluation of flake thickness as it correlates directly with the number of layers within 2H-$MoTe_2$.[45] Although the presence of the B^1_{2g} peak in Raman spectra of CVD-grown few-layered $MoTe_2$ films has been shown by various groups; to the best of our knowledge there are currently no reports where the B^1_{2g}/E^1_{2g} peak heights ratio *vs*. film thickness has been systematically investigated for CVD-grown few-layered $MoTe_2$ films. The B^1_{2g}/E^1_{2g} peak height intensity ratios depending on the film thickness are plotted in Figure 3c. In addition, the analysis of the B^1_{2g} and E^1_{2g} peak positions (broadly following the B^1_{2g}/E^1_{2g} peak height ratio) is plotted in Figure 3d showing that there is a distinctive trend with the film thickness. Both plots are in good agreement with layer thicknesses determined by AFM and with the available literature data for few-layered $MoTe_2$ obtained by mechanical exfoliation.[45] As the film thickness and number of $MoTe_2$ layers increases, the intensity of B^1_{2g} peak tends to decrease. However, there is a certain limitation for a simple evaluation of the number of layers by Raman spectroscopy: as the intensity of B^1_{2g} peak is getting suppressed, the B^1_{2g}/E^1_{2g} peak height ratio tends to plateau and becomes a relatively insensitive parameter for films with more than 7 layers. However, we found that the optical microscopy can be useful tool for assessing thicker films (Supporting Information).

Growth of few-layered 1T'-$MoTe_2$ using MoO_3 seeding layers

The 1T'-$MoTe_2$ was grown within the same CVD system and under identical reaction conditions as 2H-$MoTe_2$, except MoO_3 was used as a seeding layer instead of Mo. Figure 4a-b show a 2D topographic AFM image and the corresponding height profile collected at the step-edge between the $MoTe_2$ film and the substrate. The film thickness corresponds to 4 layers of $MoTe_2$ under assumption of roughly 0.7 nm for 1 layer of $MoTe_2$. The thickness is comparable with the initial MoO_3 film (Figure S12-13, Supporting Information). The roughness of the initial thermally deposited MoO_3 (R_q = 0.484 nm) and $MoTe_2$ (R_q = 0.480 nm) are identical when compared across scan areas of 5 μm × 5 μm (Figure 4c-d). This indicates the isomorphic transformation and suggests that the conversion is dictated by the quality of the initial seeding film and reaction conditions at optimal level.

Raman spectroscopy confirms that 1T'-$MoTe_2$ has been successfully grown,[46] with several characteristic Raman peaks present between 50 and 400 cm^{-1}: A_g modes at ~80, ~108, ~125 and ~161 cm^{-1}, a B_g mode at ~186 cm^{-1} and two final A_g modes at 251 and 265 cm^{-1} respectively (Figure 5a). The near identical peak positions and intensities of the peaks in the Raman spectra taken at 12 different locations across the film indicates the high-quality and uniformity of the 1T'-$MoTe_2$ films produced. Raman mapping based on the intensity of the characteristic A_g mode at 161 cm^{-1} reaffirms that the 1T'-$MoTe_2$ films are uniform (Figure S14, Supporting Information). Raman spectroscopy also

reveals that the entire MoO_3 film was completely converted to $MoTe_2$ as the resulting spectra do not display any peaks associated with MoO_2 and MoO_3 (Figure S15, Supporting Information).

The crystallinity of a 4-layered film was investigated using HRTEM (Figure S16a, Supporting Information) and SAED (Figure S16b, Supporting Information). The data showed that the studied film was polycrystalline with the domain size of *ca.* 10 nm. However, the results are consistent with the recent literature report on the 1T'-$MoTe_2$ films grown at a similar temperature of 650°C.[37]

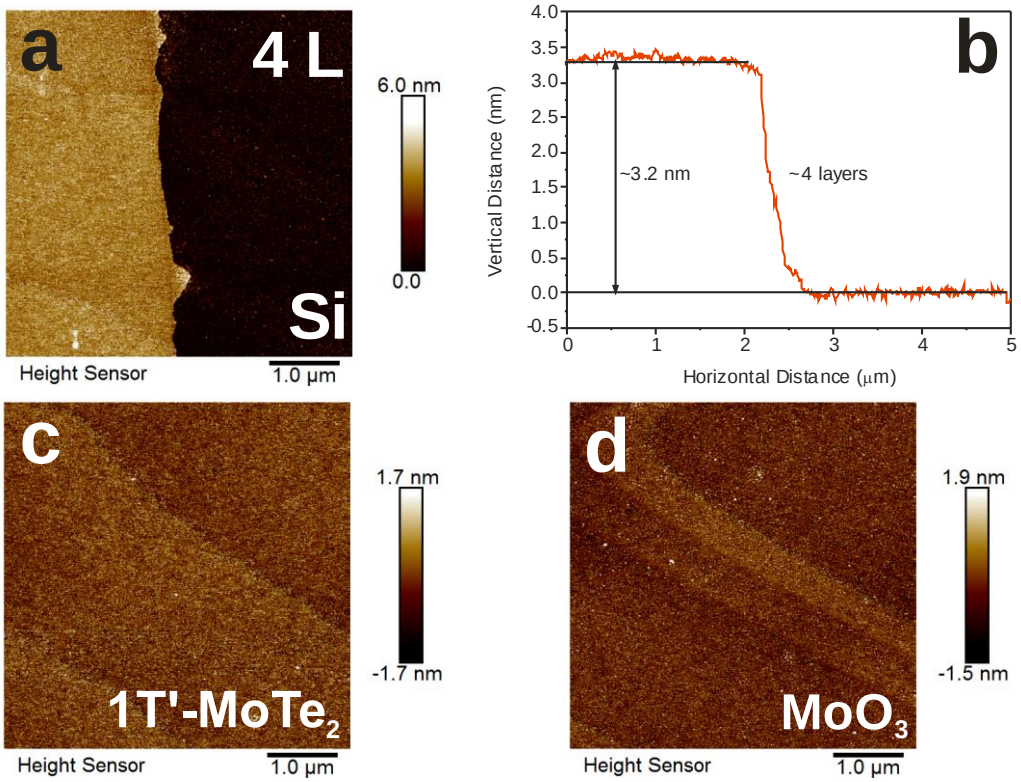

Figure 4. AFM measurement over the 5 μm x 5 μm area and a representitive 2D topographic profile of the interface between few-layered 1T'-$MoTe_2$ and SiO_2/Si substrate (a) the variation in height between the film and the substrate measured on a 4-layered $MoTe_2$ film from Figure 5a (b); 2D topographic profile of a 5 μm x 5 μm area of 4-layered $MoTe_2$ on SiO_2/Si substrate (c); 2D topographic profile of a 5 μm x 5 μm area of thermally sputtered MoO_3 film on SiO_2/Si substrate used as a seeding layer (d).

Simultaneous growth of 2H- and 1T'-$MoTe_2$

The phase selectivity of the reaction over only one type of seeding layer implies that there is an opportunity to exploit different conversion reaction kinetics of Mo and MoO_3 precursor films to $MoTe_2$ polymorphs. Therefore, a 300 nm SiO_2/Si substrate with both Mo and MoO_3 deposited onto it was converted using the same CVD setup and reaction conditions (650 °C and 30 mg of $FeTe_2$ precursor at the source) as have been discussed for the synthesis of phase pure 2H- and 1T'-$MoTe_2$. The successful simultaneous growth of both phases on the same substrate was confirmed by Raman spectroscopy with Mo converting to 2H-$MoTe_2$ and MoO_3 converting to 1T'-$MoTe_2$, respectively

(Figure 5b). An image taken from the sample shows the two phases separated by a 20 micron strip of bare SiO_2/Si substrate (Figure 5c).

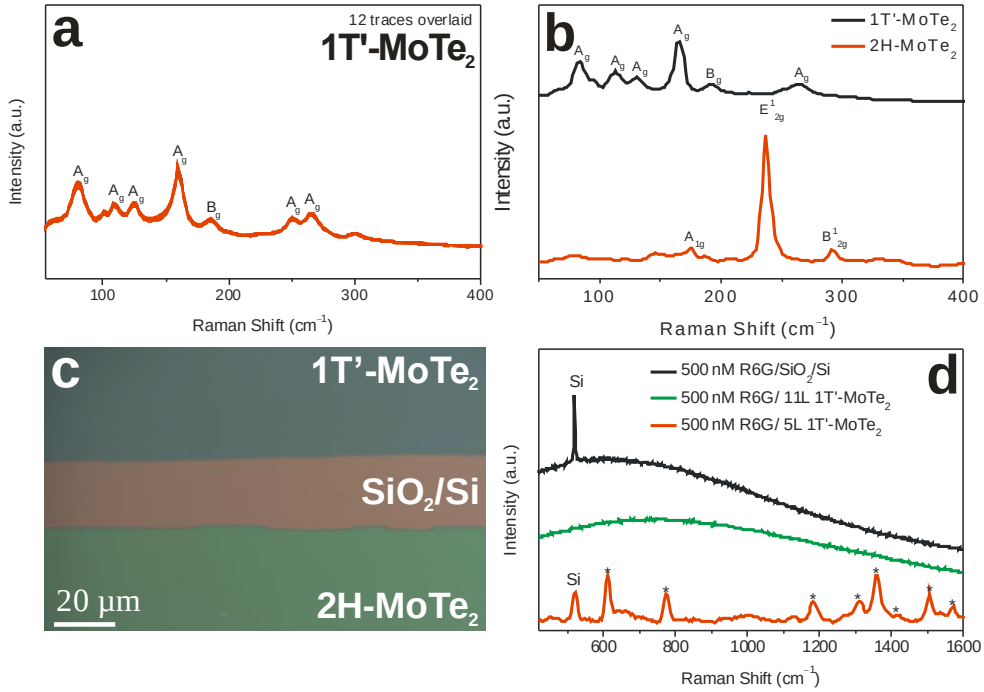

Figure 5. A 532 nm Raman spectrum from a 4L 1T'-$MoTe_2$ film on 300 nm SiO_2/Si (a); 532 nm Raman spectra from 1T'- and 2H-$MoTe_2$ grown simultaneously on 300 nm SiO_2/Si substrate (b); Image of the two $MoTe_2$ phases grown simultaneously separated by a ~20 µm strip of bare SiO_2/Si substrate for a better optical contrast (c) 532 nm Raman spectra of 500 nM solution of Rhodamine 6G drop casted on different substrates (d).

A careful assessment of the process was carried out by conducting the reactions at different flux rates, *e.g.* by using various amount of $FeTe_2$ at the source. The outcome of these studies is summarized in Figure S17. The simultaneous conversion of Mo to 2H-$MoTe_2$ and MoO_3 into 1T'-$MoTe_2$ was achieved on the same substrate and in a single reaction at low loadings of $FeTe_2$ (30 mg). We hypothesise that the lower oxidation state of Te^{-2} in $FeTe_2$ leads to the simultaneous conversion at low evaporation rates due to 1T'-$MoTe_2$ phase being kinetically stabilized at the substrate.[38] Achieving simultaneous growth in a single reaction is an important development since the method proposed here does not rely upon any post-growth modification[38,47] and is only dependent upon the nature of initial Mo and MoO_3 seed layers which are easy to control. Currently most methods for creating 1T'-2H junctions have focused on post-growth modification, involving techniques as varied as electrostatic doping, laser irradiation and the application of strain[11,38,48,49]. In this context, the access to a single step reaction may prove to be more advantageous and become widely adopted.

Few-layered 1T'-$MoTe_2$ as a sensing substrate

A preliminary study was conducted to determine if few-layered 1T'-$MoTe_2$ films grown via CVD without any further modification could act as Surface Enhanced Raman Spectroscopy (SERS) substrates using a typical dye molecule, rhodamine 6G, as a Raman probe. The R6G solution (500 nM) was dropped onto a film of 5-layer 1T'-$MoTe_2$ and a bare SiO_2/Si substrate before Raman spectra were collected from both areas (Figure 5d). The signals collected from the R6G deposited on bare SiO_2/Si exhibit a large fluorescence background and no detectable Raman peaks for R6G can be found. In contrast to this, the fluorescence is massively suppressed by the 1T'-$MoTe_2$ film and Raman features of the dye, labelled with "*", are clearly visible. It is thought that the efficient charge transfer between $MoTe_2$ and R6G decreases the fluorescence cross section and causes subsequent fluorescence quenching.[26] The use of the few-layer 1T'-$MoTe_2$ film greatly increases the signal ratio of Raman/fluorescence features allowing for the R6G Raman peaks to be clearly distinguishable from the background. However, even at a relatively small increase in number of layers from 5-layered to 11-layered 1T'-$MoTe_2$ films resulted in the complete suppression of the SERS activity (Figure 5d). Still, since 1T'-$MoTe_2$ does not have distinctive Raman modes (e.g. like phonon-active out-of-plane B^1_{2g} peak at ca. 289 cm^{-1} in 2H-$MoTe_2$) the sensing ability of few–layered samples towards R6G presents a good probe for distinguishing between atomically thin and bulk samples.

SERS is a technique routinely used to probe trace amounts of molecules; therefore, we tested the sensitivity of the technique. A set of R6G solutions were prepared with concentrations ranging from 500-0.5 nM to investigate the sensitivity of the SERS-active 1T'-$MoTe_2$ films. Figure S18 displays the Raman spectra of the R6G/1T'-$MoTe_2$ solutions depending on concentrations. Characteristic R6G Raman peaks at 612, 773, 1184, 1308, 1360, 1508, 1569, 1602 and 1646 cm^{-1} are labelled and are consistent with literature spectra. These peaks are clearly visible for the of 500 and 50 nM concentrations. For the 5 nM solution it is possible to distinguish the peaks at 612, 773 and 1360 cm^{-1} from the background, but the peaks within the 1569-1646 cm^{-1} range exhibit a significant broadening and it is no longer possible to distinguish these peaks individually. Below this concentration, individual peaks cannot be identified. Recent studies on the use of 2D materials as SERS substrates show that the enhancement factor is highly dependent upon the thickness of the 2D material.[50–52] Decreasing the thickness of a substrate leads to increasing enhancement factors.

3. Conclusions

In conclusion, we have described a viable method which is suitable for achieving preferential growth of two stable $MoTe_2$ polymorphs on the same substrate and in a single reaction. We have also demonstrated the applicability of a $FeTe_2$ precursor for the preparation of a desired polymorph under controlled conditions. In this context, the recent advancement in nanolithography technology provide the opportunity to design seeding layers to a high level of precision before the CVD process. Therefore, a single step route to the growth of a preferred $MoTe_2$ polymorph where the outcome of a CVD reaction is dictated solely by the composition of the seeding layer can help the progress in rational and reproducible design of $MoTe_2$-based systems. Hence, this method may help to advance

the adaptability of 2D chalcogenides in practical applications, such as the phase-controlled growth of metallic/semiconducting coplanar homojunctions.

4. Experimental Section

Substrates were cut using a diamond tipped scribe from a wafer of 300 nm SiO_2/Si(100) (Inseto) to a size of 10×10 mm^2. The substrates were cleaned via ultrasonication in acetone and isopropyl alcohol, spending 10 minutes in each solvent before being dried in a stream of nitrogen gas. Smaller 8×8 mm^2 were diced using a diamond saw.

Specified thicknesses of molybdenum (99.95%) were deposited on to the cleaned substrates via electron beam physical vapour deposition using a Plassys MEB550s. Deposition occurred under a vacuum of $1x10^{-6}$ mbar at a rate of 0.07 nm/s, with the electron beam gun emission current at 220 mA. The thicknesses of the molybdenum films were controlled by a quartz crystal microbalance. MoO_3 films were deposited by thermal evaporation of MoO_3 pellets (99.99%, Pi-Kem) in a Plassys MEB400 under a vacuum of $2x10^{-6}$ mbar and at a rate of 0.2 nm/s.

Chemical vapour deposition was used to synthesise the $MoTe_2$ thin films. Firstly, into a 31.5 cm quartz ampoule (inside diameter: 12 mm, outside diameter: 15 mm) was placed a 13.5 cm quartz tube (inside diameter: 9 mm, outside diameter: 11 mm) until it was resting against the end of the larger ampoule. Then the substrate was placed into the quartz ampoule until it rested against the quartz tube. Subsequently 30 - 33 mg of $FeTe_2$ powder was placed into a 7 cm long quartz ampoule (inside diameter: 9 mm, outside diameter: 11 mm) which was inserted into the large quartz ampoule until the open end rested against the substrate. The 31.5 cm ampoule was placed into a 43.5 cm quartz work tube (inside diameter: 17 mm, outside diameter: 20 mm) which itself resides inside a Lenton tube furnace. One end of the work tube was connected to a cylinder of 5% H_2/Ar carrier gas, whilst the other end was connected to a vacuum pump through which the system could be evacuated. Before the CVD process began the system was evacuated to a pressure of $2×10^{-1}$ mbar, before being refilled with the carrier gas, this procedure was carried out a total of three times to ensure an oxygen free environment for the reaction. The substrate temperature was set to 650 ˚C and source temperature with $FeTe_2$ precursor at 630^{o}C. The ramping rate was at 5 ˚C/min with a dwell time of 4 hours, before cooling to room temperature at 5 ˚C/min. A commercially available and cheap carrier gas mixture containing only 5 vol. % of H_2 in Ar was used at a flow rate of 300 sccm.

The Raman measurements were carried out in a backscattering configuration on a Horiba-JY HR800 spectrometer equipped with a solid-state green laser (λ = 532 nm). All spectra were collected unless otherwise stated through a 50× objective and dispersed by 1200 g/mm grating. The Si and sapphire most intense peaks were used as internal standards. The laser power used to irradiate samples was kept at 10 mW to avoid sample degradation and the diameter of the confocal pinhole was 100 μm.

Raman maps were measured on a WITec alpha300 R spectrometer using a 532 nm laser excitation. Spectra were collected using a 50× objective with a 1 s integration time and 1 μm spatial resolution. Background subtraction of the spectra was carried out on WITec Project 4.1 software and maps were generated based on the intensity of the peaks.

XPS spectra were collected on a system consisting of a Scienta MX650 X-ray source coupled with a Scienta RS4000 hemispherical analyser. XPS spectra were acquiring using a monochromatic Al *Kα* anode (photon energy =1486.7 eV) with a pass energy of 200 eV in the hemispherical analyser. The XPS set-up was kept at a pressure of $1x10^{-9}$ mbar and samples were attached to a copper holder and annealed at 300 ˚C under vacuum for an hour before XPS spectra were recorded to remove surface contaminants.

Transmission electron microscopy was conducted on a JEOL CFEG ARM instrument operated at 200kV, using samples supported by holey carbon films and Au grids. Selected area electron diffraction patterns were typically collected from a 20 or 50 micrometre diameter area. Beam damage was evident for the 1T' samples but not for the 2H sample after prolonged exposure to the electron beam. To remove $MoTe_2$ films from SiO_2/Si substrates, they were submersed in 10 % HF solution for ~30 s before being placed into a beaker filled with deionised water so that the $MoTe_2$ films floated on the surface. The films were then scooped up with Carbon on 200 mesh grids. Energy dispersive Xray spectroscopy (EDS) data was collected in (probe-corrected) scanning transmission electron microscopy mode, employing a Bruker X-Flash detector.

Atomic Force Microscopy (AFM) measurements were obtained using a Bruker Dimension Icon AFM. Film steps relative to the SiO_2/Si substrate were measured over a scan area of 5 μm x 5 μm. The step edges were created by using a permanent marker to draw a line ~2 mm wide across a bare SiO_2/Si substrate. Subsequently molybdenum was deposited onto the substrate, before being sonicated in isopropyl alcohol for 30 seconds to remove the marker, taking a ~2 mm thick line of molybdenum with it, hence leaving a bare area of SiO_2/Si adjacent to the deposited molybdenum film. The molybdenum film was then converted to $MoTe_2$ using the procedure described above, allowing the $MoTe_2$ film thickness to be measured against the bare line of SiO_2/Si substrate. Surface roughness measurements were also recorded over a scan area of 5 μm x 5 μm for SiO_2/Si substrate, Mo, MoO_3 and $MoTe_2$ films. A new tip was used for each sample to minimise errors associated with the AFM instrument.

Olympus BX41 microscope integrated in Horiba-JY HR800 spectrometer was used for optical imaging. All images were captured using 50x objective. Intensity of the light source (Euromex fiber optic light source EK-1, equipped with 12 V, 100 W halogen lamp) was adjusted to level 8 when capturing images for contrast measurements and to level 8.5 when capturing images for the colour palette. White balance was adjusted to R/B = 0.91:1.21 via the source settings section in LabSpec5 software when capturing contrast images. White balance was adjusted to imitate different colour temperature white light sources when capturing images for the colour palette.

Optical contrast difference was measured using ImageJ software. Colour optical images were split into RGB channels using ‘’Split Channels’’ function. Contrast profile was obtained by selecting an area in the image and then pressing ‘’K’’.

Rhodamine 6G (R6G) was diluted to 10 mM in ethanol, followed by subsequent dilution to the desired concentration in water. A 10 μL spot of diluted R6G was applied to the surface and left to dry before a gentle rinse with water and subsequent drying. SERS spectra were obtained on a WITec alpha 300R with a 532 nm laser excitation wavelength (laser power at sample 33 mW) and a 600 g/mm diffraction

grating. Spectra were acquired using a 10x objective with a 1 s integration time. Spectra averaging (of 3 spectra per sample) and baseline subtraction was carried out in WiRE 4.2 software.

Supporting Information

Supporting Information is available from the Wiley Online Library or from the author.

Acknowledgements

We acknowledge the University of Glasgow, EPSRC (EP/P001653/1), and the Carnegie Trust for a Research Incentive Grant (RIG007428) for supporting this work. T.P. thanks the FWF P27769-N20 for funding. J.P.F thanks the Energy Technology Partnership for the PECRE grant awarded.

Conflict of Interest

The authors declare no conflict of interest.

Keywords

Chemical vapour deposition; two dimensional materials; transition metal dichalcogenides; surface enhanced Raman spectroscopy; polymorphic transition

[1] Y.-H. Lee, X.-Q. Zhang, W. Zhang, M.-T. Chang, C.-T. Lin, K.-D. Chang, Y.-C. Yu, J. T.-W. Wang, C.-S. Chang, L.-J. Li, T.-W. Lin, *Adv. Mater.* **2012**, *24*, 2320.

[2] S. Najmaei, Z. Liu, W. Zhou, X. Zou, G. Shi, S. Lei, B. I. Yakobson, J.-C. Idrobo, P. M. Ajayan, J. Lou, *Nat. Mater.* **2013**, *12*, 754.

[3] J. Mann, Q. Ma, P. M. Odenthal, M. Isarraraz, D. Le, E. Preciado, D. Barroso, K. Yamaguchi, G. von Son Palacio, A. Nguyen, T. Tran, M. Wurch, A. Nguyen, V. Klee, S. Bobek, D. Sun, T. F. Heinz, T. S. Rahman, R. Kawakami, L. Bartels, *Adv. Mater.* **2014**, *26*, 1399.

[4] S. Manzeli, D. Ovchinnikov, D. Pasquier, O. V. Yazyev, A. Kis, *Nat. Rev. Mater.* **2017**, *2*, 17033.

[5] J. Zhou, J. Lin, X. Huang, Y. Zhou, Y. Chen, J. Xia, H. Wang, Y. Xie, H. Yu, J. Lei, D. Wu, F. Liu, Q. Fu, Q. Zeng, C.-H. Hsu, C. Yang, L. Lu, T. Yu, Z. Shen, H. Lin, B. I. Yakobson, Q. Liu, K. Suenaga, G. Liu, Z. Liu, *Nature* **2018**, *556*, 355.

[6] L. Liu, J. Wu, L. Wu, M. Ye, X. Liu, Q. Wang, S. Hou, P. Lu, L. Sun, J. Zheng, L. Xing, L. Gu, X. Jiang, L. Xie, L. Jiao, *Nat. Mater.* **2018**, *17*, 1108.

[7] E. Preciado, F. J. R. Schülein, A. E. Nguyen, D. Barroso, M. Isarraraz, G. Von Son, I. H. Lu, W. Michailow, B. Möller, V. Klee, J. Mann, A. Wixforth, L. Bartels, H. J. Krenner, *Nat. Commun.* **2015**, *6*, 8593.

[8] C. Palacios-Berraquero, M. Barbone, D. M. Kara, X. Chen, I. Goykhman, D. Yoon, A. K. Ott, J. Beitner, K. Watanabe, T. Taniguchi, A. C. Ferrari, M. Atatüre, *Nat. Commun.* **2016**, *7*, 12978.

[9] J. Shi, X. Wang, S. Zhang, L. Xiao, Y. Huan, Y. Gong, Z. Zhang, Y. Li, X. Zhou, M. Hong, Q. Fang, Q. Zhang, X. Liu, L. Gu, Z. Liu, Y. Zhang, *Nat. Commun.* **2017**, *8*, 958.

[10] Y.-Q. Bie, G. Grosso, M. Heuck, M. M. Furchi, Y. Cao, J. Zheng, D. Bunandar, E. Navarro-Moratalla, L. Zhou, D. K. Efetov, T. Taniguchi, K. Watanabe, J. Kong, D. Englund, P. Jarillo-Herrero, *Nat. Nanotechnol.* **2017**.

[11] Y. Wang, J. Xiao, H. Zhu, Y. Li, Y. Alsaid, K. Y. Fong, Y. Zhou, S. Wang, W. Shi, Y. Wang, A. Zettl, E. J. Reed, X. Zhang, *Nature* **2017**, *550*, 487.

[12] D. H. Keum, S. Cho, J. H. Kim, D. H. Choe, H. J. Sung, M. Kan, H. Kang, J. Y. Hwang, S. W. Kim, H. Yang, K. J. Chang, Y. H. Lee, *Nat. Phys.* **2015**, *11*, 482.

[13] L. Reeves, Y. Wang, T. F. Krauss, *Adv. Opt. Mater.* **2018**, 1800272.

[14] A. Li, Q. Chen, P. Wang, Y. Gan, T. Qi, P. Wang, F. Tang, J. Z. Wu, R. Chen, L. Zhang, Y. Gong, *Adv. Mater.* **2018**, *31*, 1805656.

[15] Z. Lu, Y. Xu, Y. Yu, K. Xu, J. Mao, G. Xu, Y. Ma, D. Wu, J. Jie, *Adv. Funct. Mater.* **2020**, 1907951.

[16] H. Fang, J. Liu, H. Li, L. Zhou, L. Liu, J. Li, X. Wang, T. F. Krauss, Y. Wang, *Laser Photonics Rev.* **2018**, *12*, 1800015.
[17] H. Fang, J. Liu, Q. Lin, R. Su, Y. Wei, T. F. Krauss, J. Li, Y. Wang, X. Wang, *Adv. Opt. Mater.* **2019**, 1900538.
[18] Y. Qi, P. G. Naumov, M. N. Ali, C. R. Rajamathi, W. Schnelle, O. Barkalov, M. Hanfland, S.-C. Wu, C. Shekhar, Y. Sun, V. Süß, M. Schmidt, U. Schwarz, E. Pippel, P. Werner, R. Hillebrand, T. Förster, E. Kampert, S. Parkin, R. J. Cava, C. Felser, B. Yan, S. A. Medvedev, *Nat. Commun.* **2016**, *7*, 11038.
[19] B. Yan, C. Felser, *Annu. Rev. Condens. Matter Phys. is* **2017**, *8*, 337.
[20] J. Jiang, Z. K. Liu, Y. Sun, H. F. Yang, C. R. Rajamathi, Y. P. Qi, L. X. Yang, C. Chen, H. Peng, C. C. Hwang, S. Z. Sun, S. K. Mo, I. Vobornik, J. Fujii, S. S. P. Parkin, C. Felser, B. H. Yan, Y. L. Chen, *Nat. Commun.* **2017**, *8*, 13973.
[21] P. Tsipas, S. Fragkos, D. Tsoutsou, C. Alvarez, R. Sant, G. Renaud, H. Okuno, A. Dimoulas, *Adv. Funct. Mater.* **2018**, 1802084.
[22] S. Hussain, S. A. Patil, D. Vikraman, N. Mengal, H. Liu, W. Song, K.-S. An, S. H. Jeong, H.-S. Kim, J. Jung, *Sci. Rep.* **2018**, *8*, 29.
[23] J. C. McGlynn, I. Cascallana-Matías, J. P. Fraser, I. Roger, J. McAllister, H. N. Miras, M. D. Symes, A. Y. Ganin, *Energy Technol.* **2018**, *6*, 345.
[24] P. Zhuang, Y. Sun, P. Dong, W. Smith, Z. Sun, Y. Ge, Y. Pei, Z. Cao, P. M. Ajayan, J. Shen, M. Ye, *Adv. Funct. Mater.* **2019**, *29*, 1901290.
[25] J. C. McGlynn, T. Dankwort, L. Kienle, N. A. G. Bandeira, J. P. Fraser, E. K. Gibson, I. Cascallana-Matías, K. Kamarás, M. D. Symes, H. N. Miras, A. Y. Ganin, *Nat. Commun. 2019 101* **2019**, *10*, 1.
[26] L. Tao, K. Chen, Z. Chen, C. Cong, C. Qiu, J. Chen, X. Wang, H. Chen, T. Yu, W. Xie, S. Deng, J. Bin Xu, *J. Am. Chem. Soc.* **2018**, *140*, 8696.
[27] B. E. Brown, *Acta Crystallogr.* **1966**, *20*, 268.
[28] J. D. Cain, F. Shi, J. Wu, V. P. Dravid, *ACS Nano* **2016**, *10*, 5440.
[29] S. Li, Y. Lin, W. Zhao, J. Wu, Z. Wang, Z. Hu, Y. Shen, D. Tang, J. Wang, Q. Zhang, H. Zhu, L. Chu, W. Zhao, C. Liu, Z. Sun, T. Taniguchi, M. Osada, W. Chen, Q. Xu, *Nat. Mater.* **2018**.
[30] A. Koma, K. Sunouchi, T. Miyajima, *Microelectron. Eng.* **1984**, *2*, 129.
[31] J. Kim, C. Bayram, H. Park, C. W. Cheng, C. Dimitrakopoulos, J. A. Ott, K. B. Reuter, S. W. Bedell, D. K. Sadana, *Nat. Commun.* **2014**, *5*, 4836.
[32] J. Zhou, F. Liu, J. Lin, X. Huang, J. Xia, B. Zhang, Q. Zeng, H. Wang, C. Zhu, L. Niu, X. Wang, W. Fu, P. Yu, T. Chang, C. Hsu, D. Wu, H. Jeng, Y. Huang, H. Lin, Z. Shen, C. Yang, L. Lu, K. Suenaga, W. Zhou, T. Pantelides Sokrates, G. Liu, Z. Liu, *Adv. Mater.* **2016**, *29*, 1603471.
[33] J. H. Sung, H. Heo, S. Si, Y. H. Kim, H. R. Noh, K. Song, J. Kim, C. S. Lee, S. Y. Seo, D. H. Kim, H. K. Kim, H. W. Yeom, T. H. Kim, S. Y. Choi, J. S. Kim, M. H. Jo, *Nat. Nanotechnol.* **2017**, *12*, 1064.
[34] L. Zhou, A. Zubair, Z. Wang, X. Zhang, F. Ouyang, K. Xu, W. Fang, K. Ueno, J. Li, T. Palacios, J. Kong, M. S. Dresselhaus, *Adv. Mater.* **2016**, *28*, 9526.
[35] L. Zhou, K. Xu, A. Zubair, X. Zhang, F. Ouyang, T. Palacios, M. S. Dresselhaus, Y. Li, J. Kong, *Adv. Funct. Mater.* **2017**, *27*, 1603491.
[36] S. J. Yun, G. H. Han, H. Kim, D. L. Duong, B. G. Shin, J. Zhao, Q. A. Vu, J. Lee, S. M. Lee, Y. H. Lee, *Nat. Commun.* **2017**, *8*, 2163.
[37] X. Xu, S. Chen, S. Liu, X. Cheng, W. Xu, P. Li, Y. Wan, S. Yang, W. Gong, K. Yuan, P. Gao, Y. Ye, L. Dai, *J. Am. Chem. Soc.* **2019**, *141*, 2128.
[38] Y. Yoo, Z. P. DeGregorio, Y. Su, S. J. Koester, J. E. Johns, *Adv. Mater.* **2017**, *29*, 1605461.
[39] C. Ruppert, O. B. Aslan, T. F. Heinz, *Nano Lett.* **2014**, *14*, 6231.
[40] T. H. Fleisch, G. J. Mains, *J. Chem. Phys.* **1982**, *76*, 780.
[41] Y. V. Plyuto, I. V. Babich, I. V. Plyuto, A. D. Van Langeveld, J. A. Moulijn, *Appl. Surf. Sci.* **1997**, *119*, 11.
[42] C. H. Naylor, W. M. Parkin, J. Ping, Z. Gao, Y. R. Zhou, Y. Kim, F. Streller, R. W. Carpick, A. M. Rappe, M. Drndić, J. M. Kikkawa, A. T. C. Johnson, *Nano Lett.* **2016**, *16*, 4297.
[43] C. D. Wagner, *Handbook of x-ray photoelectron spectroscopy: a reference book of standard data for use in x-ray photoelectron spectroscopy, Physical Electronics Division, Perkin-Elmer Corp.*; Physical Electronics Division Perkin-Elmer Corp.: Eden Prairie Minn., 1979.
[44] J. H. Huang, K. Y. Deng, P. S. Liu, C. T. Wu, C. T. Chou, W. H. Chang, Y. J. Lee, T. H. Hou, *Adv. Mater. Interfaces* **2017**, *4*, 1700157.
[45] M. Yamamoto, S. T. Wang, M. Ni, Y. F. Lin, S. L. Li, S. Aikawa, W. Bin Jian, K. Ueno, K. Wakabayashi, K. Tsukagoshi, *ACS Nano* **2014**, *8*, 3895.

[46] L. Zhou, S. Huang, Y. Tatsumi, L. Wu, H. Guo, Y. Q. Bie, K. Ueno, T. Yang, Y. Zhu, J. Kong, R. Saito, M. Dresselhaus, *J. Am. Chem. Soc.* **2017**, *139*, 8396.
[47] R. Ma, H. Zhang, Y. Yoo, Z. P. Degregorio, L. Jin, P. Golani, J. Ghasemi Azadani, T. Low, J. E. Johns, L. A. Bendersky, A. V. Davydov, S. J. Koester, *ACS Nano* **2019**, *13*, 8035.
[48] S. Cho, S. Kim, J. H. Kim, J. Zhao, J. Seok, D. H. Keum, J. Baik, D.-H. Choe, K. J. Chang, K. Suenaga, S. W. Kim, Y. H. Lee, H. Yang, *Science (80-.).* **2015**, *349*, 625.
[49] S. Song, D. H. Keum, S. Cho, D. Perello, Y. Kim, Y. H. Lee, *Nano Lett.* **2016**, *16*, 188.
[50] C. Qiu, H. Zhou, H. Yang, M. Chen, Y. Guo, L. Sun, *J. Phys. Chem. C* **2011**, *115*, 10019.
[51] X. Ling, W. Fang, Y. H. Lee, P. T. Araujo, X. Zhang, J. F. Rodriguez-Nieva, Y. Lin, J. Zhang, J. Kong, M. S. Dresselhaus, *Nano Lett.* **2014**, *14*, 3033.
[52] Y. Lee, H. Kim, J. Lee, S. H. Yu, E. Hwang, C. Lee, J. H. Ahn, J. H. Cho, *Chem. Mater.* **2016**, *28*, 180.